Nucleic Acids Research Advance Access published September 18, 2009

Nucleic Acids Research, 2009, 1–15
doi:10.1093/nar/gkp697

Tertiary network in mammalian mitochondrial $tRNA^{Asp}$ revealed by solution probing and phylogeny

Marie Messmer[1], Joern Pütz[1], Takeo Suzuki[2], Tsutomu Suzuki[2], Claude Sauter[1], Marie Sissler[1] and Florentz Catherine[1,*]

[1]Architecture et Réactivité de l'ARN, Université de Strasbourg, CNRS, IBMC 15 rue René Descartes, 67084 Strasbourg, France and [2]Department of Chemistry and Biotechnology, Graduate School of Engineering, University of Tokyo, 7-3-1 Hongo, Bunkyo-ku, Tokyo 113-8656, Japan

Received May 25, 2009; Revised July 23, 2009; Accepted August 7, 2009

ABSTRACT

Primary and secondary structures of mammalian mitochondrial (mt) tRNAs are divergent from canonical tRNA structures due to highly skewed nucleotide content and large size variability of D- and T-loops. The nonconservation of nucleotides involved in the expected network of tertiary interactions calls into question the rules governing a functional L-shaped three-dimensional (3D) structure. Here, we report the solution structure of human mt-$tRNA^{Asp}$ in its native post-transcriptionally modified form and as an *in vitro* transcript. Probing performed with nuclease S1, ribonuclease V1, dimethylsulfate, diethylpyrocarbonate and lead, revealed several secondary structures for the *in vitro* transcribed mt-$tRNA^{Asp}$ including predominantly the cloverleaf. On the contrary, the native $tRNA^{Asp}$ folds into a single cloverleaf structure, highlighting the contribution of the four newly identified post-transcriptional modifications to correct folding. Reactivities of nucleotides and phosphodiester bonds in the native tRNA favor existence of a full set of six classical tertiary interactions between the D-domain and the variable region, forming the core of the 3D structure. Reactivities of D- and T-loop nucleotides support an absence of interactions between these domains. According to multiple sequence alignments and search for conservation of Leontis–Westhof interactions, the tertiary network core building rules apply to all $tRNA^{Asp}$ from mammalian mitochondria.

INTRODUCTION

Transfer RNAs (tRNAs) constitute key molecules in protein biosynthesis in all living organisms. To fulfill their biological role, they have specific structural properties allowing interactions with several partners such as their cognate aminoacyl-tRNA synthetases (aaRSs), elongation factor, mRNA or ribosome (1). Presently, several thousands of tRNA sequences are known (2). A vast majority of them fold into the canonical cloverleaf secondary structure, and furthermore into a three-dimensional (3D) functional L-shape as first revealed by the crystal structure of $tRNA^{Phe}$ (3,4). Transition from 2D to 3D structure is supported by nine tertiary interactions involving conserved and semi-conserved residues that are localized within the D- and the T-loops, and within the core of the molecule (connector regions, D-stem and variable region). The tertiary interaction network is conserved in bacterial, archaeal and eukaryal cytosolic tRNAs. It involves nucleotides which either form atypical base-pairs or triple interactions, the latter made either of three remote nucleotides or of a Watson–Crick pair and an additional distant nucleotide (5,6).

A major unanswered question, however, concerns the 3D folding rules for mammalian mitochondrial tRNAs (mt-tRNAs) for which sequences are not canonical. Sequence comparison of these tRNAs, in addition to the description of typical characteristics of secondary structures, highlighted 'bizarre' features (7). Exceptionally of $tRNA^{Ser(AGY)}$ is missing the full D-domain and $tRNA^{Ser(UCN)}$ has an extended anticodon stem. Mammalian mt-tRNAs present other unprecedented size variations in both D- and T-loops and lack a number of conserved and semi-conserved residues essential to

*To whom correspondence should be addressed. Tel: +33 3 88 41 70 59; Fax: +33 3 88 60 22 18; Email: C.Florentz@unistra.fr

the establishment of a canonical tertiary interaction network. Only four families ($tRNA^{Leu(UUR)}$, $tRNA^{Leu(CUN)}$, $tRNA^{Gln}$ and $tRNA^{Asn}$) show strong conservation of the nine potential classical tertiary interactions, including those between the D- and T-loops, and may thus well fold into the canonical L-fold (7). For all other families, a gradual disappearance of the theoretical tertiary interactions is observed; in extreme examples only three of them can be predicted (7). A few mammalian mt-tRNAs have been investigated experimentally for their 3D structural features. Two atypical $tRNA^{Ser(UCN)}$ (8,9) and $tRNA^{Ser(AGY)}$ (10) have been studied by enzymatic and chemical structure probing in solution, and a nuclear magnetic resonance (NMR) structure was established for $tRNA^{Ser(AGY)}$ (missing the D-domain) (10). Transient electric birefringence experiments showed that the angle between the two branches of the 'L' is more obtuse for these two tRNAs and for human mt-$tRNA^{Lys}$ than for classical tRNAs (120°–140° as compared to 70°–90° respectively) (11,12). In the single case of bovine mt-$tRNA^{Phe}$, solution mapping experiments with enzymatic and chemical probes lead to 3D structural information on a moderately diverging 'bizarre' mt-tRNA (13). In this tRNA, the presence of the six expected tertiary interactions within the core of the tRNA is supported experimentally and the absence of conserved nucleotides G18G19 and T54ΨCG57 in the D- and T-loops, respectively, leads to the absence of interaction between the corresponding domains at the corner of the expected 'L' fold.

For a refined understanding of the rules that govern the folding of mammalian mt-tRNAs, we have tackled the case of human mt-$tRNA^{Asp}$ by structural mapping in solution with enzymatic and chemical probes. This tRNA has already been investigated to determine the identity signals responsible for specific aspartylation by human mt-AspRS (14). The number of such signals is severely reduced in comparison with $tRNA^{Asp}$ from other kingdoms: only two important elements in the anticodon triplet are maintained and the discriminator nucleotide G73 is lost, suggesting a strongly degenerated set of identity elements in mammalian mt aspartylation systems (14). This observation prompted us to search for concomitant structural alteration of the tRNA, in order to gain some insight into structure/function evolution of aminoacylation systems in mitochondria. Experiments were performed on both native tRNA extracted from HeLa cells and human placenta, containing all the post-transcriptional modifications, as well as on the corresponding *in vitro* transcript.

Here, the set of post-transcriptional modifications of native human mt-$tRNA^{Asp}$ has been defined and a cloverleaf retrieved as secondary structure. However, a combination of three alternate secondary structures, including a cloverleaf, a cloverleaf with a large loop and an extended bulged hairpin, has been discovered for the *in vitro* transcribed RNA, demonstrating the high contribution of post-transcriptional modifications to structure the mt-tRNAs. Reactivities in native tRNA toward structural probes are in favor (i) of the existence of an extensive tertiary network of interactions forming the core of an L-shaped structure and (ii) of the absence of interactions between the D- and T-loops. The relevance of the rules governing the tertiary network of human mt-$tRNA^{Asp}$ applied to other mammalian mt-tRNAs is discussed in terms of conservation of Leontis–Westhof interaction patterns in the six core tertiary interactions.

MATERIALS AND METHODS

Materials

Diethylpyrocarbonate (DEPC), aniline, hydrazine, TRI REAGANT®, 5′-biotinylated oligonucleotide and streptavidin-coated beads were purchased from Sigma-Aldrich. Nuclease T1 used for enzymatic structure probing was from Stratagene, nuclease S1 as well as ribonuclease V1 were from PIERCE. Dimethylsulfate (DMS) was bought from Acros Organics. RNase T1 used for mass spectrometric analyses was purchased from EPICENTRE Biotechnologies. Acrylonitrile was purchased from Wako Pure Chemical Industries. [γ-^{32}P]ATP (3000 Ci/mmol) was from Amersham.

Mass spectrometric analysis of the post-transcriptional modifications in human mt-$tRNA^{Asp}$

Mt-$tRNA^{Asp}$ purified from human placenta as described previously (15,16) was provided by Dr. Yohei Kirino (Univ. of Pennsylvania). The sequence of a synthetic 3′-biotinylated DNA for the chaplet column chromatography was 5′-taagatatataggatttagcctataattta-3′. The purified $tRNA^{Asp}$ (250 fmol) was digested by RNase T1 or RNase A, and then analyzed by capillary liquid chromatography (LC)/nano electrospray ionization mass spectrometry (nanoESI-MS) as described (17). A linear ion trap-orbitrap hybrid mass spectrometer (LTQ Orbitrap XL, Thermo Fisher Scientific) was equipped with a custom-made nanospray ion source and a splitless nano HPLC system (DiNa, KYA Technologies). Cyanoethylation was carried out according to the literature (18) with slight modifications. Reaction mixture (16 µl) consisting of 1 µl of 1 µM $tRNA^{Asp}$, 13 µl of 1.1 M triethylammonium acetate (pH 7.0) with 41% ethanol and 2 µl of acrylonitrile was incubated at 70°C for 2 hours. After cyanoethylation, the mixture was lyophilized and dissolved with water. Half the amount was digested by RNase T1, then subjected to the LC/nanoESI-MS analysis.

Structural mapping in solution

Native tRNA was prepared from HeLa cell mitochondria according to established procedures. Total mitochondrial tRNAs were extracted by using the TRI REAGANT® method following the manufacturer's procedure. Specific mitochondrial $tRNA^{Asp}$ was isolated from total tRNAs as previously described in (19,20) by hybridization to a 5′-biotinylated oligonucleotide bound to streptavidin coated beads and complementary to 34 nt at the 5′-end of the tRNA. The gene for human mt-$tRNA^{Asp}$ has been cloned previously (21) including a hammerhead ribozyme (22) and tRNA sequence downstream of the

T7 polymerase promoter. A BstNI site was inserted coincidental with the 3′-end of the tRNA sequence, which allows the synthesis of tRNA ending with the expected CCA sequence. *In vitro* transcription was performed as described in (21) with adequate amounts of T7 RNA polymerase (purified according to ref. 23). After phenol extraction, the transcript was purified on denaturing 12% polyacrylamide/8 M urea gels, electroeluted and ethanol-precipitated.

Structural mapping of tRNAs was done using enzymatic (nuclease S1, specific for single-stranded region and ribonuclease V1, specific for duplex or highly structured region) and chemical (DMS, specific for N3 of cytosine, DEPC, specific for N7 of adenosine, and lead (Pb^{2+}), specific for single-stranded regions) probes. [^{32}P]-labeling of the tRNA transcript 5′-end and the subsequent purification of tRNA molecules from polyacrylamide gels were carried out as described earlier (24). Before structural probing, transcripts were denatured by heating at 60°C in H_2O and slowly cooled down to room temperature.

Enzymatic probing. Digestion with nuclease S1 or ribonuclease V1 were performed as described (24). Briefly, transcripts were incubated in 50 mM HEPES-KOH pH 7.5, 10 mM $MgCl_2$ and 25 mM KCl for 5 min at 25°C. For digestion with S1 nuclease, 1 mM $ZnCl_2$ was added. Reaction mixtures (10 µl) contained 30 000 Cerenkov c.p.m. of transcript supplemented with 2 µg of unlabeled *Escherichia coli* total tRNA and either 12.8 U nuclease S1 or $3.6.10^{-2}$ U RNase V1. Cleavage reactions were performed during 5 min at 25°C and were stopped by adding 1 vol of 0.6 M AcONa pH 5, 3 mM EDTA and 0.1 mg/ml *E. coli* total tRNA followed by ethanol precipitation.

Chemical probing. Modification of N7 atoms of guanosine residues and of N3 atoms of cytosine residues by DMS, and modification of N7 positions of adenosine by DEPC were done according to established procedures (25). Optimal concentration of chemicals and incubation times for mt-tRNA transcripts were chosen as described (24). Under native conditions, DMS reactions were for 10 min at 25°C in 50 mM HEPES-NaOH pH 7.5, 5 mM $Mg(OAc)_2$, 50 mM K(OAc) and 2 mM β-mercaptoethanol. Semi-denaturing conditions were for 5 min at 25°C in 50 mM HEPES-NaOH pH 7.5, 50 mM K(OAc), 1 mM EDTA and 2 mM β-mercaptoethanol. Denaturing conditions were for 30 s at 60°C in 50 mM HEPES-NaOH pH 7.5 and 1 mM EDTA. DEPC modification was as with DMS but incubation times were 10 and 20 min for native and semi-denaturing conditions and 5 s for the denaturing one. Cleavage reactions were performed for 10 min in the dark at 60°C using 10 µl of a modified aniline solution (100 µl 1 M aniline, 60 µl CH_3COOH and 930 µl H_2O). Concerning the DMS, the cleavage reaction was preceded by a second modification using 10 µl hydrazine 50% (v/v in water) for 5 min in the dark. Between all the modification and the cleavage steps, tRNAs were ethanol precipitated. All cleavage products were analyzed on denaturing polyacrylamide gels as described below.

Cleavage by $Pb(OAc)_2$ was performed as described in (26). Briefly, transcripts were incubated in 50 mM HEPES-NaOH pH 7.5, 5 mM $Mg(OAc)_2$ and 50 mM K(OAc) for 10 min at 25°C. A freshly prepared $Pb(OAc)_2$ solution in water was added to final concentrations of 5 and 25 mM. Samples (10 µl) were incubated at 25°C for 5 min. Reactions were stopped by cooling on ice, adding EDTA to a final concentration of 33 mM and ethanol precipitated. Control without probe was run in parallel.

Assignment of cleavage positions. Alkaline ladders were performed by incubation of labeled transcripts (30 000 Cerenkov c.p.m.) and 2 µg of total tRNA from *E. coli* in 50 mM $NaHCO_3$ pH 9, at 80°C for 8 min. Guanine ladders were obtained by incubation of labeled transcripts in 10 mM Na-citrate pH 4.5, 3.2 M urea, 0.4 mM EDTA and 2 µg of unlabeled *E. coli* total tRNA for 4 min at 60°C followed by the addition of 2 U RNase T1 and a second incubation at 60°C for 4 min. The products of the probing reactions were analyzed on 12% polyacrylamide/8 M urea denaturing gels. Controls without probes but supplemented with $ZnCl_2$ were run in parallel on each gel.

Mt-tRNA^{Asp} 3D modeling

A 3D model of human mt-tRNA^{Asp} was built on the basis of the crystallographic structure of *E. coli* tRNA^{Asp} in complex with AspRS (PDB id: 1C0A) (27). Sequence changes as well as base and phospho-ribose backbone manipulations were performed with 'O' (28) and 'assemble' (http://www.bioinformatics.org/assemble/ -ref. 29), and conjugate-gradient minimization (500 cycles in restrained Cartesian mode) of the model (including hydrogen atoms) was performed with CNS (30). Figures of the 3D model were prepared with PyMol (31).

RESULTS

Background

Figure 1A recalls nucleotides involved in the network of tertiary interactions sustaining classical tRNA 3D structures (tRNAs from bacteria, archae, eukaryotic cystosol; ref. 5,6). Nine interactions are present. Most of the network takes place in the core of the molecule, namely in the D-arm and the variable region, involving nucleotides which either form a pair at long-distance (i.e. R15-Y48, N26-N44 with R for purine, Y for pyrimidine, N for any nucleotide), or which form triples. Triples involve either a base pair formed along the secondary structure and a single nucleotide at distance (i.e. 9/12-23, 13-22/46, 45/10-25), or 3 nt unrelated in the secondary structure (i.e. U8-A14-A21). Three further interactions involve the T- and D-loops, one interaction within the T-loop (T54-A58) and two interactions bringing the two loops close to each other (G18-Ψ55, G19-C56), to form the elbow of the 'L'. Mammalian mt-tRNA^{Asp} (Figure 1B) deviate from canonical tRNAs by sizes of D- and T-loops and by the lack of several conserved and semi-conserved residues essential to the establishment of the tertiary interaction network. Strategic nucleotides, especially nucleotides G18 and G19 in the D-loop, and nucleotides

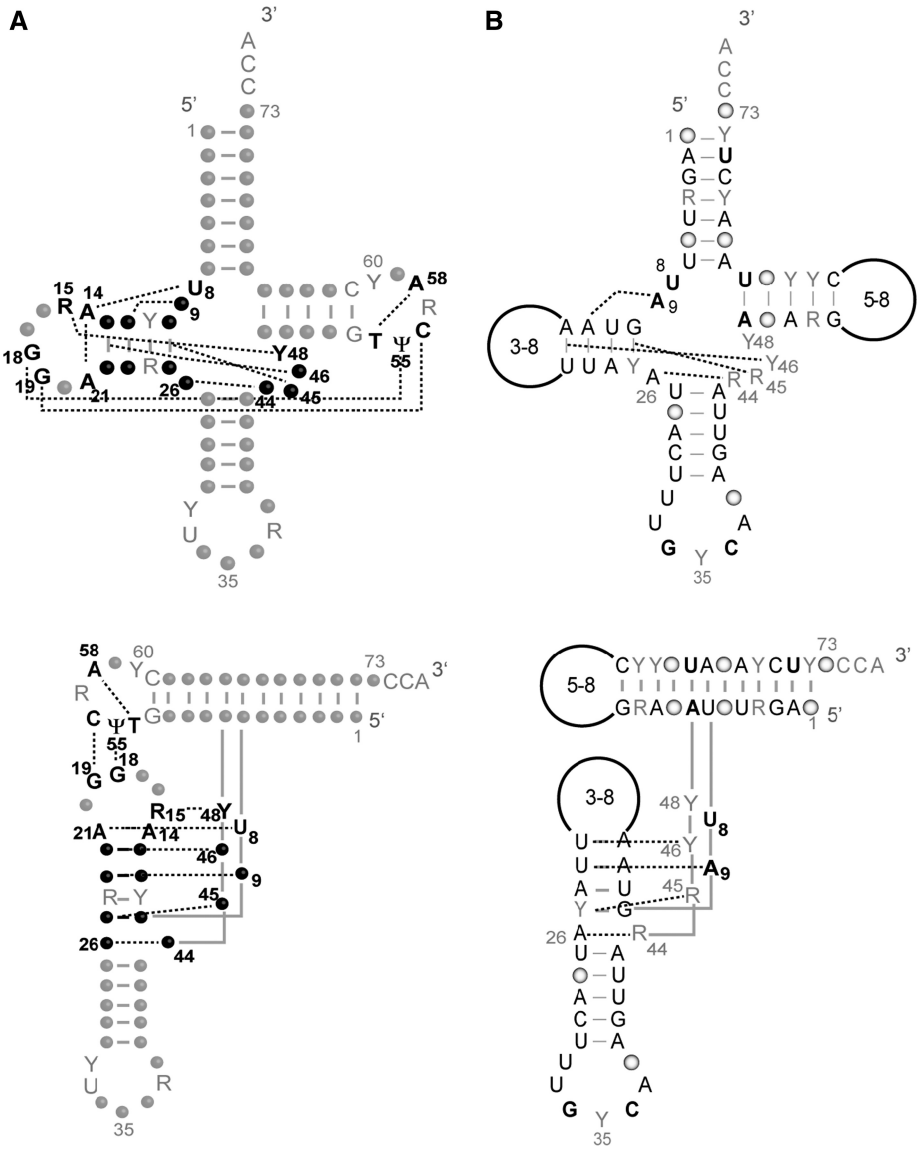

Figure 1. Tertiary interaction networks in tRNAs. (**A**) Canonical tRNA (e.g. bacterial, archaeal, eukaryotic cytosolic). Data are according to crystallographic structures (5,6). Nucleotide positions involved in the nine tertiary interactions are indicated in bold. They are either strictly conserved, semi-conserved (Y for pyrimidine, R for purine) or not conserved (black dots) and bring together secondary structural domains (top) into an L-shaped 3D fold (bottom). Other strictly conserved or semi-conserved nucleotides are indicated in gray. Numbering is according to (2). Residues 8, 9 and 26 are considered as connectors between domains. (**B**) Mammalian mitochondrial tRNA^{Asp}. The displayed 'typical' secondary and tertiary interactions have been compiled under 'Mamit-tRNA' data (http://mamit-trna.u-strasbg.fr/, 32) by alignment of 136 sequences. Nucleotides in black and bold characters are strictly conserved. Those indicated in black are conserved to ≥90%. Dominance of a given nucleotide in ≥50% and ≤90% of sequences as well as semi-conservation (Y or R) is indicated in grey. Conservation ≤50%, is represented by open circles. Due to large size and sequence variations in D- and T-loops, no sequence conservation can be indicated. Four tertiary interactions can be predicted in the core of the molecule. No interaction between the D- and T-loops can be anticipated in any mitochondrial tRNA^{Asp} sequence.

U54U55C56 of the T-loop are absent, leaving the question open of the existence of any interaction between these loops. By analogy to classical tRNAs, only four potential tertiary interactions in the core of the 3D structure would be conserved when the full set of available mammalian mitochondria sequences of tRNA^{Asp} are considered (7,32) (Figure 1B). Among them, the existence of the triple interaction A9/A12-U23 has recently been experimentally confirmed while investigating the effects of myopathy-related mutation A7526G (A9G) on structure and aminoacylation properties of mt-tRNA^{Asp} (33).

Post-transcriptional modifications in human mt-tRNA^{Asp}

Native mt-tRNA^{Asp} (Figure 2A) was isolated from human placenta by the chaplet column chromatography (15,16). To determine species and positions of the post-transcriptional modifications, human mt-tRNA^{Asp} was digested by RNase T1 or RNase A into fragments, and analyzed by a highly accurate and sensitive method of RNA mass spectrometry (capillary LC/nanoESI-MS) (17). As shown in Figure 2B and Table 1, we could detect negatively-charged ions of 15 digestion fragments

produced by RNase T1 and RNase A digestions that cover the whole sequence of mt-tRNA^{Asp}. According to the observed values of singly or multiply charged ions, the exact molecular masses of the RNA fragments with or without modifications could be unambiguously determined (Table 1). Each fragment was further analyzed by a MS/MS experiment using collision-induced dissociation (CID) to position the detected modifications in the tRNA sequence. The MS/MS analysis of fragment No. 4 (Table 1) determined 1-methyladenosine (m^1A) at position 9 and N^2-methylguanosine (m^2G) at position 10 (Figure 2C). These two modifications are conserved at the corresponding positions in several animal mt-tRNAs (tRNAdb, (2), http://trnadb.bioinf.uni-leipzig.de/). We also found m^2G at position 10 occurred partially as observed in the CID spectrum of fragment No. 4′ (UAUUm^1AGp) (Figure 2C). Judging from the peak area in the mass chromatogram, about 50 % of G10 is modified to m^2G10 (Figure 2B). The anticodon-containing fragment (No. 1) showed a molecular mass of 27-mer RNA containing a wobble modification of queuosine (Q). As it is known that Q is a modified G that is resistant to RNase T1 digestion (34), Q can be assigned at position 34 in principle. We also observed partial modification of Q34 (~10%), resulting in the detection of the 21-mer RNA (No. 1′) which was cleaved at position 34 by RNase T1 (Figure 2B and Table 1). For detecting mass-silent pseudouridine (Ψ), Ψ in tRNA^{Asp} was cyanoethylated by acrylonitril treatment, prior to RNase T1 digestion. We found the fragment No 1′ increased in molecular mass by 53 Da, indicating a single Ψ to be present in this fragment. In the CID spectrum of the cyanoethylated RNA fragments No. 1′ (Figure 2D), the quadruply charged product ion w8′ (m/z 669.8212) exactly matched with the m/z value containing cyanoethylated-Ψ. On the contrary, in the CID spectrum of nonderivatized No. 1′ (Figure 2D), we detected the related product ion w8 (m/z 656.5684) which corresponds to the unmodified RNA fragment. Besides, other product ions of 3′-termini including y1, y3, w4 and w5 are commonly found in both CID spectra. These data demonstrate that Ψ was placed at position 27. In summary, human mt-tRNA^{Asp} has Ψ27, m^1A9, m^2G10 and Q34 as its post-transcriptional modifications (Figure 2A).

Enzymatic and chemical solution structure of native human mitochondrial tRNA^{Asp}

Structure probing in solution is based upon the reactivity of RNA molecules toward chemicals or enzymes that have a specific target on RNA (35–37). Probes are used under statistical conditions where less than one cleavage or modification occurs per molecule. In the present work, accessibility of the human mt-tRNA^{Asp} has been probed under native conditions by nucleases specific for single-stranded (nuclease S1) and double-stranded or structured regions (ribonuclease V1). While the use of these enzymatic probes allows deciphering of the overall secondary structure of the RNA, a more precise investigation at the atomic level involves the chemical probes DMS, DEPC and Pb^{2+}. DEPC modification at N7 position of adenine residues and DMS modification at N3 position of cytosine residues can be detected by strand scission with aniline. If these atoms are accessible and reactive in the RNA 3D structure, they are detected under native conditions. If they are involved in secondary or tertiary structural elements, they are non-reactive under native conditions but become detectable under semi-denaturing and fully denaturing conditions.

Probing experiments have been performed at 25°C on 5′- or 3′-end labeled tRNA molecules. Cleavage fragments were revealed on denaturating 12% polyacrylamide gels. Representative autoradiograms of enzymatic cleavage of native tRNA^{Asp} (with post-transcriptional modifications) are presented in Figure 3A. Complete data resulting from extensive probing with both enzymatic and chemical probes are summarized on a cloverleaf structure (Figure 3B). Control incubations without probes confirmed the intrinsic weakness of human mt-tRNAs at pyrimidine-A bonds as already described for tRNA^{Lys} (24) and tRNA$^{Leu(UUR)}$ (38). All degradations are annotated on the autoradiograms as well as on the cloverleaf structure. For technical reasons, residues 1–10 and 74–76 could not be investigated.

Analysis of nucleotide reactivities to chemical probes and of phosphodiester bonds to enzymatic probes within native tRNA^{Asp} unambiguously reveals a classical cloverleaf. Typical reactivities correspond to strong cleavages by single-strand specific nuclease S1 all along residues 14–20 (corresponding to the D-loop), residues 32–35 (anticodon loop), residues 44 and 45 (variable region) and residues 55 and 56 (T-loop), as well as cleavages by the double-strand specific ribonuclease V1 all along nucleotides 28, 29 (anticodon stem), 43 (end of anticodon stem/entry of variable region), nucleotides 62–65 (T-arm) and nucleotides 69, 70 and 72 (acceptor arm). Significant alkylation by DMS under native conditions, as revealed by direct strand scission, is observed at the N3 position of residues C16 and C20 (D-loop), C36 (anticodon loop) and C54 (T-loop), whereas residues C26 (D-arm), C30 (anticodon arm) and C61 and C62 (T-arm) are not reactive under native conditions (not shown). These residues become fully reactive under denaturing conditions. Reactivities of adenosines to DEPC under native conditions are strong for residues A21 (D-loop), A37 and A38 (anticodon loop) and A56 and A57 (T-loop), while residues A11–A13 (D-arm), A28 and A29 (anticodon arm) and A49, A51 and A64 (T-arm) are not reactive. However, some reactivities do not fit. The phosphodiester bond 5′ to nucleotide C20 (D-loop) is cut by ribonuclease V1.

Unfortunately, the corresponding cleavage product co-migrates with the product of degradation between residues C20 and A21, therefore no conclusion about the involvement of residue C20 within a tertiary interaction can be proposed. Moreover, residues A12 and A13 (D-arm) are reactive towards the single-strand specific nuclease S1.

Nucleotides within D- and T-loops deserve particular attention. In the D-loop, all phosphodiester bonds are cleaved by single-strand specific enzymatic probe, two major degradations occur, and atomic positions of bases

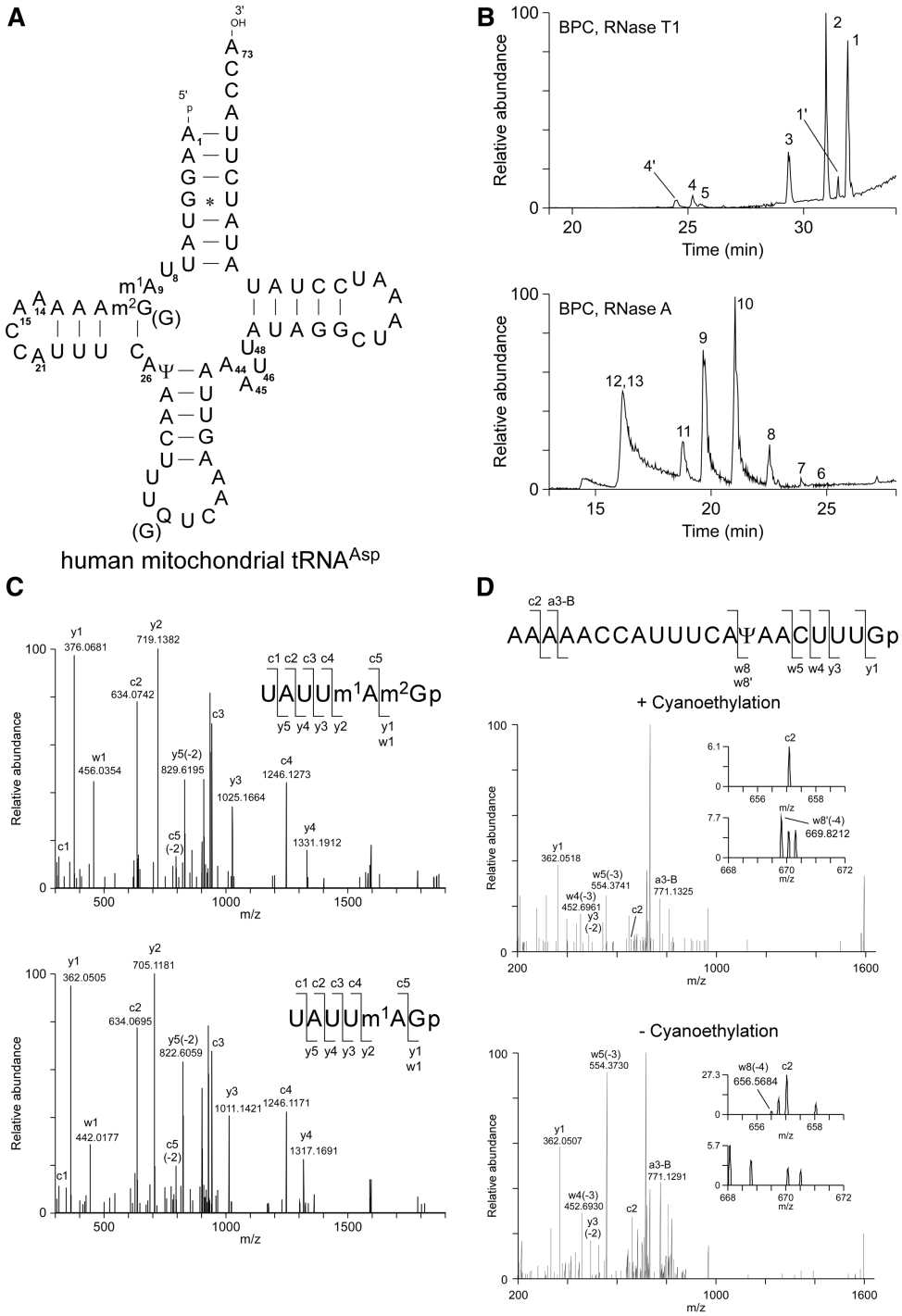

Figure 2. Post-transcriptional modifications in human mt-tRNA^{Asp} (**A**) Secondary structure of human mt-tRNA^{Asp} (53) with modifications determined in this study. Abbreviations are used as follows: m^{1}A, 1-methyladenosine; m^{2}G, N^2-methylguanosine; Ψ, pseudouridine; Q, queuosine. 5′-terminus 'p' and 3′-terminus 'OH' represent monophosphate and hydroxy group, respectively. (**B**) Base peak chromatograms (BPC) of RNA fragment analyses of human mt-tRNA^{Asp} digested by RNase T1 (upper panel) and RNase A (lower panel). Each fragment is numbered in the chromatograms as described in Table 1. (**C**) Collision induced dissociation (CID) spectra of UAUUm^{1}Am^{2}Gp (upper panel) and UAUUm^{1}AGp (lower panel). Precursor ions were *m*/*z* 982.6 and 975.6, respectively. Product ions, whose nomenclatures are mentioned by (76), are indicated in each spectrum and on the sequence of each fragment. The charge state of product ions is indicated in parentheses. (**D**) CID spectra of AAAAACCAUUUCAΨAACUUUGp with (upper panel) or without (lower panel) cyanoethylation. Precursor ions *m*/*z* 747.9 (with cyanoethylation, upper panel) and *m*/*z* 742.2 (without cyanoethylation, lower panel) were used for CID, respectively. The product ion containing cyanoethylated pseudouridine(s) is marked with a prime notation. The insets show expanded ranges for *m*/*z* 655–659 and 668–672, respectively including monoisotopic w8(-4) and w8′(-4) ions.

Table 1. List of RNA fragments from human mitochondrial $tRNA^{Asp}$ detected by MS analysis

No	Sequences of RNA fragments	Molecular mass	Monoisotopic *m/z*		Charge state
			Observed	Calculated	
	RNase T1 fragments				
1	AAAAACCAUUUCAΨAACUUUQUCAAAGp	8756.213	795.0098	795.012	−11
1′	AAAAACCAUUUCAΨAACUUUGp	6686.873	741.9777	741.978	−9
2	CUAAAUCCUAUAUAUCUUACCA (3′ terminus)	6848.915	683.9017	683.884	−10
3	UUAAAUUAUAGp	3538.447	706.6801	706.682	−5
4	UAUUm^{1}Am^{2}Gp	1967.270	982.6292	982.627	−2
4′	UAUUm^{1}Agp	1953.255	975.6188	975.619	−2
5	pAAGp (5′ terminus)	1101.129	1100.1222	1100.122	−1
	RNase A fragments				
6	m^{1}Am^{2}GAAAAACp	2670.446	1334.2153	1334.215	−2
7	pAAGGUp (5′ terminus)	1752.202	875.0916	875.093	−2
8	AAAGUp	1656.241	827.1147	827.113	−2
9	AGGCp	1342.199	670.0933	670.092	−2
10	AAAUp	1311.193	654.5911	654.589	−2
11	AACp	981.157	980.1503	980.149	−1
12	AUp or AΨp	653.088	652.0830	652.081	−1
13	ACp	652.104	651.0989	651.097	−1

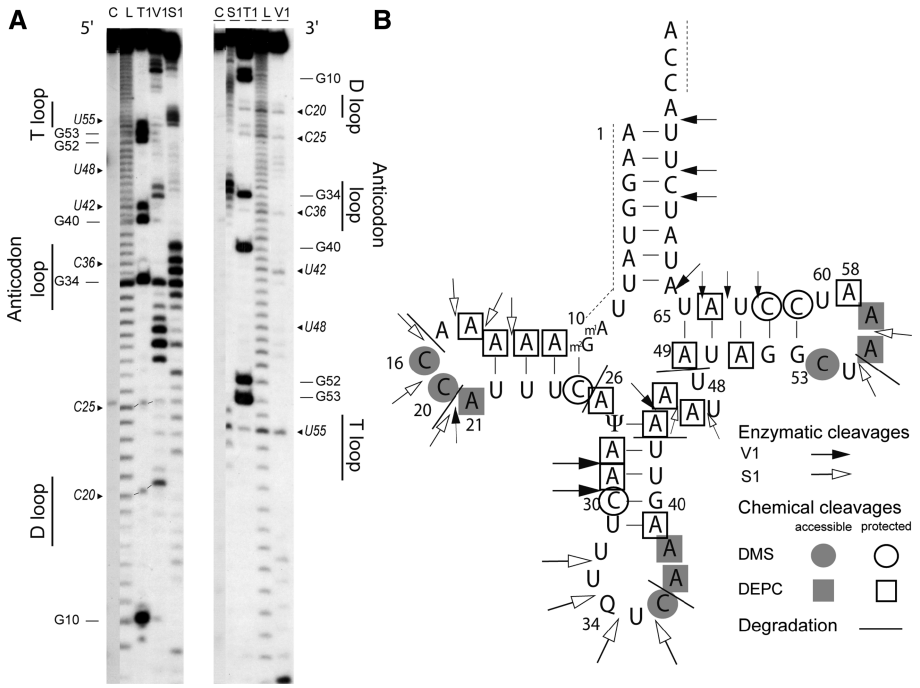

Figure 3. Solution structural mapping of human native mitochondrial $tRNA^{Asp}$, extracted from HeLa cells. (**A**) Autoradiograms of typical polyacrylamide gels on which ribonuclease V1 and nuclease S1 enzymatic cleavage products were mapped. tRNA was either 5′-end (left panel) or 3′-end (right panel) labeled with [^{32}P]. C: control incubation in the absence of probes, L: alkaline degradation, T1: G-ladder under denaturing conditions, V1 and S1: cleavage in presence of either structural probe under native conditions (see 'Materials and Methods' section). Numbering of nucleotides and theoretical secondary domains are given on both sides of the panels. Chemically fragile phosphodiester bonds at Y-A stretches are indicated in italics with the name of the 5′Y nucleotide. (**B**) Reactivities to enzymatic and chemical (autoradiograms not shown) probes under native conditions presented on the theoretical cloverleaf secondary structure of mt-$tRNA^{Asp}$. For detailed legend, see inset. For enzymatic probes, the size of the arrows is proportional to cleavage intensity.

are reactive to chemical probes. Accordingly, the possibility of interaction of this loop with another domain of the RNA is restrained. T-loop nucleotides are also very reactive to both single-strand specific enzyme and to chemical probes. Further, degradation at U55/A56 is strong. Accordingly, the T-loop nucleotides are not protected against structural probes by any neighboring RNA domain. Nonreactivity of several atomic positions to chemical probes can be interpreted by intrinsic folding of either loop. N7 of A58 is likely to reflect a stacking with neighboring nucleotides C54 and/or U55. The present data are not in support of D- and T-loop interactions. The absence of reactivity of N7 A14 fits with an interaction with residue U8 through a Hoogsteen interaction as

in classical tRNAs (6). Reactivity of N7 A21 to DEPC under native conditions is in agreement with interaction of residues A14 and A21 in a way not involving the Hoogsteen side.

The D-stem and variable region of mt-tRNA^{Asp} are rich in adenosine residues. None of these adenosines (A11–A14, and A44–A46) is reactive to DEPC under native conditions. Accordingly, their N7 atoms are involved in a higher-order structure. They can be protected against DEPC either due to stacking with neighboring bases and/or due to hydrogen bonding within tertiary interactions. Nonreactivity of N7 A45 supports an involvement in the triple interaction G10-C25/A45 and non-reactivity of N7 A46 with an involvement in the triple A13-U22/A46. Nonreactivity of N7 of A26 and A44 is in agreement with their involvement in stacking.

Enzymatic and chemical solution structure of *in vitro* transcribed human mitochondrial tRNA^{Asp}

Probing experiments on *in vitro* transcribed mt-tRNA^{Asp} have been performed using the same enzymatic and chemical probes as for native tRNA, under similar conditions. In addition, reactivity to Pb^{2+} has been investigated. Representative autoradiograms and the full set of reactivities under native conditions are summarized on the theoretical cloverleaf structure (Figure 4A1 and A2). Control incubations without probes confirmed the intrinsic higher sensitivity of the transcript as compared to native tRNA extracted from human cells, at pyrimidine-A bonds (as already described in 24,38). These degradations are annotated along the autoradiograms as well as localized on the cloverleaf structure. As was the case for the native tRNA, reactivities of residues 1–9 and 74–76 could not be observed.

Comparing the cleavage pattern of this molecule to native tRNA^{Asp}, the same reactivities of residues A28 to C30, U32 to U41 and C61 to A73 towards enzymatic (nuclease S1 and ribonuclease V1) and chemical probes (DMS and DEPC) can be observed and are therefore compatible with a secondary cloverleaf structure. Reactivity of the variable region nucleotides to chemical probing (N7 of A44 and A45 are reactive to DEPC and A44 to U47 are sensitive to the Pb^{2+}) is also consistent with this secondary structure. However, the other nucleotides display a mixture of opposite reactivities. Thus, the D-arm can be either be structured or open. A11 to A13 and U22 to U24 are cut by the double-strand specific ribonuclease V1 but also by the single-strand specific nuclease S1 and are sensitive to the lead probe. It should also be noticed that residues G10 and C25 are also cleaved by the two latter probes. Along the same trend, N7 atoms of residues A11 to A13 are reactive to DEPC. Two incompatible cleavage patterns within the theoretical D-loop are also observed. While N7 of adenosine and N3 of cytosine are reactive toward single-strand specific probes, nucleotides A14–A21 are reactive to Pb^{2+} and nucleotide A14 to nuclease S1, ribonuclease V1 cuts can be observed for all the nucleotides belonging to the loop (A14–A21). Two residues of the anticodon arm (U42 and A43) are reactive not only to RNase V1 (in agreement with the presence of an arm) but also to Pb^{2+}. In addition, N7 of A43 is reactive to DEPC. Contradictions of these types are also observed in the T-arm. On one the one hand, nucleotides A49–A51 and C62–A64 are cleaved by ribonuclease V1 and N7 atoms of residues A49 and A64 as well as N3 atoms of residues C61 and C62 are not reactive toward chemical probes. On the other hand, A49 and U50 are sensitive to nuclease S1 and N7 of A51 is reactive to DEPC. Finally, reactivities of the N3 of C53 as well as the N7 of A55 and A56 toward the chemical probes, C53–A55 toward the Pb^{2+} and A55 and A56 toward the nuclease S1 are in agreement with the presence of a T-loop. Reactivity of N7 position of residue A58 to DEPC under semi-denaturing conditions and discrete cleavage by ribonuclease V1 of A55 are in agreement with an internal loop interaction (between A58 and C54). Considering all these data, it can be concluded that the *in vitro* transcribed mt-tRNA^{Asp} mainly folds into a secondary cloverleaf structure but alternative structures are also present. Figure 4B presents two possible alternative folds to the cloverleaf, namely a cloverleaf with an open D-domain and an extended hairpin structure.

Database analysis

A set of 136 mammalian mt-tRNA^{Asp} sequences is available in the specific mammalian mt-tRNA database Mamit-tRNA (32). Figure 1B shows the most typical combination of nucleotides present in this group of molecules. A large variability in D- and T-loop size is observed. A more detailed analysis reveals three main types of D-loop sequences (5′-AAA-3′; 5′-AAYYA-3′; 5′-AAYAA-3′) (Y for pyrimidines) and three main types of T-loop sequences (5′-TGAAAAT-3′; 5′-TYAAAYY-3′; 5′-TTTA AAT-3′). Whatever the combination of the facing loops, no obvious Watson–Crick interaction can be drawn. Structural weaknesses of D-/T-loops interaction are not likely to be compensated within the tRNA itself, in contrast to various internal compensations observed in a number of highly bizarre tRNAs from animal mitochondria (39–41).

With regard to core interactions, the existence of four out of the six tertiary interactions appears possible, with most typical sequences A26–R44, G10–Y25/R45; A12–U23/A9; A13–U22/Y46. Considering a more detailed analysis of these core interactions within mt-tRNA^{Asp} families in different mammalian super-order/orders allows a fine tuned view (Supplementary Data). In all families, conservation of nucleotides is highly significant, although not absolute. This is in support of a strong contribution of tertiary interactions within the core to drive the folding of mammalian mt-tRNA^{Asp}. To search in a finer way for conservation of tertiary interactions, the set of the six candidate interactions in the core has been analyzed according to the Leontis–Westhof rules of nucleotide interactions (42). These rules propose a classification and nomenclature of nucleoside interactions found in crystal structures, according to the ‘edges’ participating in the interaction and to the orientation of the glycosidic bonds relative to the hydrogen bonds. This format allows identification of pairs that co-vary or interchange in

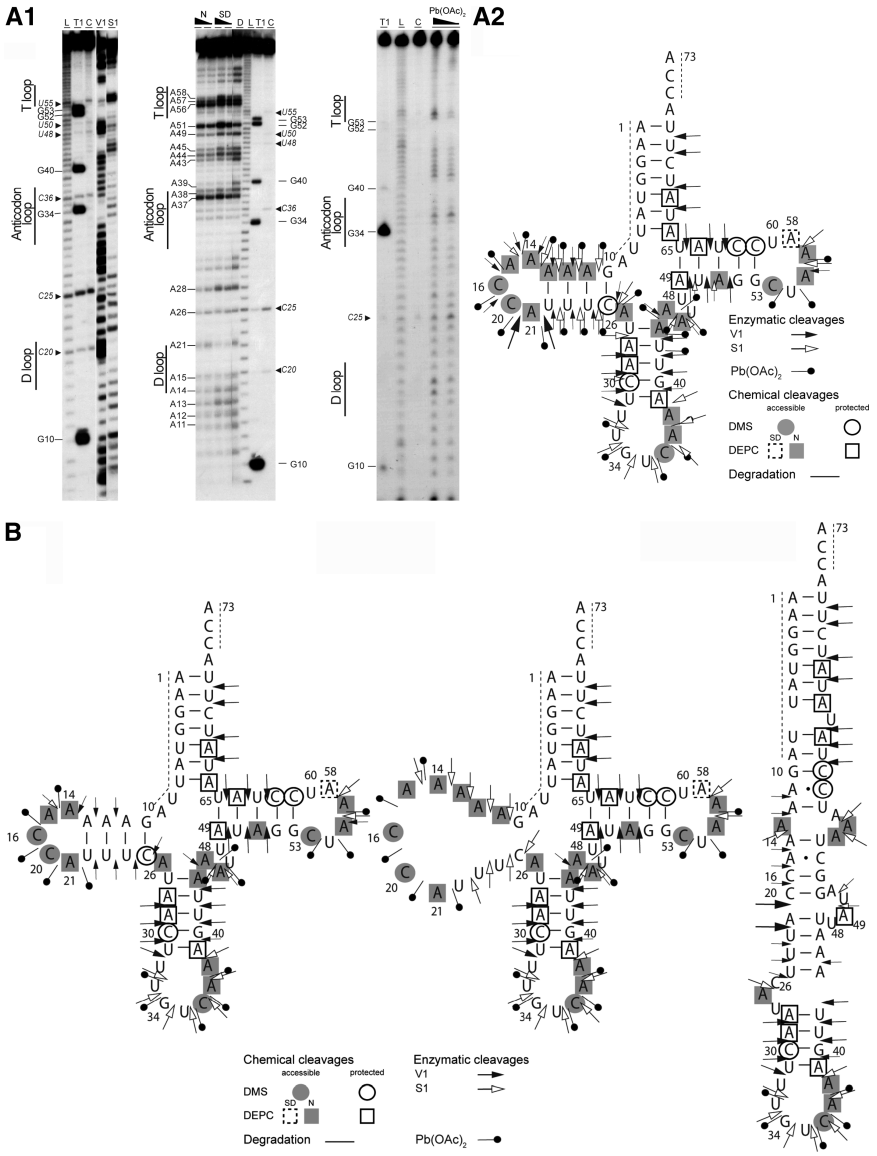

Figure 4. Solution structure probing of *in vitro* transcribed human mt-tRNA^{Asp}. (**A**) Experimental results. (A1) Autoradiograms of typical polyacrylamide gels for enzymatic mapping with ribonuclease V1 and nuclease S1 (left), chemical probing with DEPC (center) and $Pb(OAc)_2$ (right). tRNA was 5′-end [^{32}P]-labeled and submitted to denaturation at 60°C and further renaturation before submission to probes under native conditions (see 'Materials and Methods' section). C: control incubation in the absence of probes, L: alkaline degradation, T1: G-ladder under denaturing conditions, V1 and S1: cleavage in presence of either structural probes, N and SD in the central panel correspond to decreasing amounts of DEPC under native and semi-denaturing conditions, respectively, two concentration of $Pb(OAc)_2$ have also been used. Numbering of nucleotides and theoretical secondary domains are given along the panels. Chemically fragile phosphodiester bonds at Y-A stretches are indicated in italics with the name of the 5′Y nucleotide. (A2) Theoretical secondary structure cloverleaf with all observed reactivities to probes. For detailed legend, see inset. For enzymatic probes, the size of the arrows is proportional to cleavage intensity. (**B**) *In vitro* transcribed human mt-tRNA^{Asp} exists under several conformations. Reactivity to enzymatic and chemical probes are in strong support of the existence of alternative conformations. Their sorting out reveals at least two alternative structures to the cloverleaf (left), namely a cloverleaf with an open D-stem (center) and an extended bulged hairpin (right).

sequence between homologous molecules while maintaining the 3D topology. Table 2 summarizes the six core interaction schemes (involving 16 nt) in the 136 mammalian mt-tRNA^{Asp} sequences and their comparison to interaction patterns found in classical tRNAs. As an outcome, 98.3% of interactions are strictly conserved, in strong support for the existence of the full set of classical tertiary interactions in the core of mammalian mt-tRNA^{Asp}. These interactions in the core domain are depicted in the Supplementary Data.

DISCUSSION

In vitro transcribed mt-tRNA^{Asp} folds into a variety of secondary structures

Enzymatic and chemical probing of the *in vitro* transcribed human mt-tRNA^{Asp} reflects the existence of alternative structures. In addition to the dominant classical cloverleaf, large nucleotide stretches cleaved by nuclease S1 or by lead, and with reactivity to chemical probes under native conditions suggest a

Table 2. Tertiary interaction schemes in mammalian mt-tRNA^{Asp}

Tertiary Interaction		Yeast tRNA^{Phe}		*E. coli* tRNA^{Asp}		Human mt-tRNA^{Asp}		Mammalian mt-tRNA^{Asp}		
		Seq	Interaction	Seq	Interaction	Seq	Interaction	Seq	Interaction	Hits
15–48		G-C		G-C		A-U		A-U		114
								A-C		10
								G-C		7
								U-U		3
								C-U		1
								U-A		1
8–14–21	**21–14**	A-A		A-A		A-A		A-A		87
								C-A		16
								A-U		13
								U-A		12
								A-C		8
	14–8	A-U		A-U		A-U		A-U		121
								U-U		13
								C-U		2
	21–8	A-U		A-U		A-U		A-U		101
								C-U		23
								U-U		12[a]
13–22–46	**22–13**	G-C		G-C		U-A		U-A		129
								A-U		4
								G-U		1
								A-A		1
								C-A		1
	22–46	G-G		G-G		U-U		U-U		126
								A-U		4
								U-C		2
								A-A		1
								G-G		1
								A-G		1
								C-U		1
9–12–23	**23–12**	A-U		A-U		U-A		U-A		133
								A-U		3
	23–9	A-A		A-A		U-A		U-A		133
								A-A		3
10–25–45	**25–10**	C-G		U-G		C-G		C-G		108
								U-G		24
								U-A		4
	10–45	G-G		G-G		G-A		G-A		89
								G-G		40
								G-U		7[b]
								A-A		4
26–44		G-A		A-G		A-G		A-A		131
								G-A		3
								C-A		1
								A-U		1

[a]This noncompatible combination of nucleotides (U21-U8) is typically found in *Chiroptera* tRNAs where the D-loop is only 3 nt long.
[b]Residue 45 is randomly a pyrimidine : one case in *Afrotheria* mt-tRNAs and six distant cases in *Euarchontoglires* tRNAs.
The set of six tertiary interactions present in the crystallographic structures of yeast tRNA^{Phe} (3) and *E. coli* tRNA^{Asp} (27) are reported according to the Leontis–Westhof interaction code (42). The nucleotide combinations present at identical positions in human mt-tRNA^{Asp} and further in the full set of mammalian mt-tRNA^{Asp} present in Mamit-tRNA data base (http://mamit-trna.u-strasbg.fr/) (32) have been retrieved. The possibility of their interaction as in the two crystallographic structures has then been searched for in the Leontis–Westhof tables (42). The code for interaction is the following: trans Watson–Crick/Watson–Crick, *cis* Watson–Crick/Watson–Crick, *cis* Watson–Crick/Sugar Edge, *trans* Watson–Crick/Hoogsteen, *trans* Watson–Crick/Sugar Edge, *trans* Hoogsteen/Hoogsteen, *cis* Hoogsteen/Sugar Edge, not present in Leontis–Westhof tables.

version with an unstructured D-domain. A further fold corresponds to an extended hairpin. In comparison to the initial cloverleaf, this structure maintains the 7 bp of the acceptor stem and part of the anticodon domain. On the contrary, the D- and T-domains are totally refolded with numerous interdomain base pairs. The existence of alternate structures of *in vitro* transcripts has already been observed for other human mt-tRNAs (43,44). This situation was first characterized for $tRNA^{Lys}$ that does not adopt a cloverleaf but two alternative extended hairpins. In this case, the occurrence of a cloverleaf requires the presence of modified nucleotides (24,45). A single methyl group at position 9 (m^1A9) is of major importance in this process since it hinders base pairing of nucleotide 9 with nucleotide 64 in the T-stem (this can also be achieved by mutating A9 to C, or U64 to A or C). All these variants show cloverleaf-type probing patterns and are aminoacylated by human lysyl-tRNA synthetase while the wild-type transcript is not (45,46). Single-molecule FRET analysis revealed that the wild-type *in vitro* transcribed mt-$tRNA^{Lys}$ exists in a conformational equilibrium between cloverleaf and hairpin structures and that methylation of residue A9 controls this equilibrium in favor of an active cloverleaf (47,48). Enzymatic and chemical probing experiments conducted on *in vitro* transcribed $tRNA^{Ile}$ (49) and $tRNA^{Leu(UUR)}$ (38,50,51) confirmed the folding of these molecules into a secondary cloverleaf structure but further showed that they could additionally adopt alternative structures such as a cloverleaf with open D- and anticodon stems for the $tRNA^{Leu(UUR)}$ (38). The corresponding 'floppy' tertiary structure of the anticodon arm in the expected L-shaped $tRNA^{Leu(UUR)}$ becomes converted into a functional tRNA upon interaction with the cognate aminoacyl-tRNA synthetase (52). *In vitro* transcribed $tRNA^{Tyr}$ however, preferentially folds into the cloverleaf (26). This is in-line with the ranking of human mt-tRNAs into two families according to the DNA-strand on which they are encoded, both strands being highly skewed in nucleotide composition (53). $tRNA^{Tyr}$ is a G-rich, 'heavy', human mt-tRNA and consequently folds into a more stable structure than the highly A-, U- and C-rich 'light' tRNAs including the aforementioned $tRNA^{Lys}$, $tRNA^{Ile}$ and $tRNA^{Leu(UUR)}$ (7). The present data on human mt-$tRNA^{Asp}$ solution structures are a new example demonstrating the intrinsic structural plasticity of 'light' mt-tRNAs (primary sequence of this tRNA includes 29A, 24U, 11C and 7G residues).

Post-transcriptional modifications restrict the 2D folding space to a single cloverleaf

Human mt-$tRNA^{Asp}$ presents four post-transcriptional modifications, namely m^1A9, m^2G10, Ψ27 and Q34. Some of these modifications are only present partially, i.e. all copies of the tRNA are not modified at all positions, suggesting the existence of several 'modivariants' (54), as already observed for other human mt-tRNAs (20). m^1A9 is typical for mt-tRNAs and is very rare in other tRNAs (2,55). As discussed above, an unprecedented structural role for this modification was revealed along studies of human mt-$tRNA^{Lys}$ where the methyl group hinders Watson–Crick base-pairing of residue 9 with residue 64 (in the T-stem) and thus hinders folding of the RNA into an extended hairpin (24,45). m^1A9 was also shown to be crucial for structure and function of nematode mt-tRNAs lacking the entire T-arm (56). If this methyl group is inserted by the newly discovered methylase activity of human mt-RNase P (57) remains an open question. m^2G10 is a frequent modification in many tRNA families, which does not hinder Watson–Crick interaction (2,55). Ψ27 is present in about 20% of all tRNAs and stabilizes the base-pairing with A43 (58) and is present in many mt-tRNAs (2,55). The contribution of Ψ27 to mt-tRNA stability has been explicitly demonstrated for bovine mt-$tRNA^{Met}$ (59). Interestingly also, the absence of Ψ27 and Ψ28 in human cytosolic and mt-tRNAs has been correlated to sideroblastic anemiae due to an inactive pseudouridine synthase (60). Finally, Q34 is a G modification present in the anticodon loop of eukaryal and bacterial tRNAs (2,55). It is also present in a few mt-tRNAs from which $tRNA^{Asp}$ from *Asterias amurensis*, *Didelphis virginiana* and *Rattus norvegicus*. We report here its first description in a human mt-tRNA. This modification is likely involved in codon reading (61).

The enzymatic and chemical structure probing performed on native, post-transcriptionally modified, human mt-$tRNA^{Asp}$ extracted from HeLa cells reveals a perfect fit between nucleotide reactivities and a cloverleaf 2D folding (Figure 3). These data, different from those found for the corresponding *in vitro* transcript, illustrate the role of the post-transcriptional modifications in the achievement of functional $tRNA^{Asp}$ molecules in human mitochondria. Contribution of post-transcriptional modifications to tRNA folding and stability is well established with examples in different kingdoms of life and in mt-tRNAs (62–64).

Classical tertiary interactions in the core but not in D/T loop interactions, define the 3D structure of native mt-$tRNA^{Asp}$

Secondary elements of native human mt-$tRNA^{Asp}$ appear well defined. The predicted stems (acceptor arm, D-, anticodon and T-stems) are reactive to double-strand specific enzymatic probe and non reactive to chemical probes. The predicted loops react in an opposite way, i.e. strong cleavages by the single-strand specific enzymatic probe and high reactivity toward chemical probes. Two main domains of the potential 3D structure have to be considered in regard to tertiary interactions. D- and T-loop nucleotides are strongly reactive to probes, not in support of interactions between these loops. However, the reactivity of some nucleotides from both loops fits with a possible role in the tertiary network, according to rules established for classical tRNAs. Reactivities are compatible for the following interactions: A14–U8, A21–A14 and A58–C54 (or A58–U55). Reactivities of residues within the variable domain and of residue 26 are compatible with the following triples: G10–C25/A45, A13–U12/A46

and A26–A44. The existence of triple 9/12–23 has been previously supported experimentally, combining a structural and functional mutagenic approach (33). Only interaction between residues 15 and 48 could not be tested (reactivity of residue 15 is poisoned by a systematic degradation of the 15–16 phosphodiester bond and U48 is not sensitive to the probes used herein).

In summary, chemical and enzymatic probing performed herein is concordant with probing performed on classical tRNAs (65) and can be interpreted by at least five out of the six expected tertiary interactions taking place in the core domain of the tRNA, involving the D-domain and the variable region. These findings are strengthened by compilation of 136 mammalian mt-tRNA^{Asp} sequences, which revealed a high conservation in nucleotides within the core domain of the tRNA (see Supplementary Data). Moreover, more than 98% of nucleotide combinations in the full set of 16 nt involved in the six core interactions are compatible with conservation of Leontis–Westhof interaction types (Table 2). Accordingly, the six tertiary interactions can exist and are conserved in mammalian mt-tRNA^{Asp}. A 3D graphics model of human mt-tRNA^{Asp} has been built accordingly, on the basis of the crystallographic structure of *E. coli* tRNA^{Asp} in complex with the cognate aspartyl-tRNA synthetase (27). Figure 5 presents the model and highlights the predicted interactions in the core of the molecule. It also illustrates the main absence of interactions between the D- and T-loops.

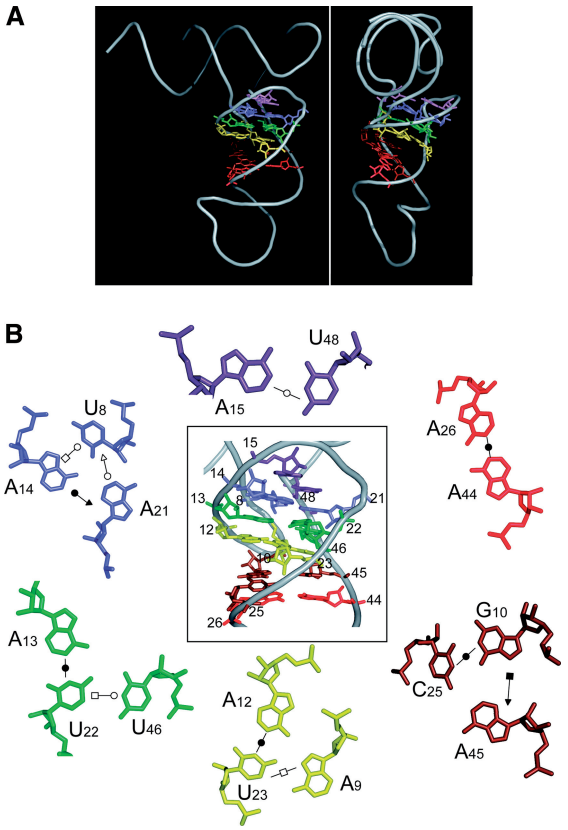

Figure 5. 3D structure model for native human mt-tRNA^{Asp}. The model has been built on the basis of crystallographic structure of *E. coli* tRNA^{Asp} in complex with its cognate aspartyl-tRNA synthetase (27). Nucleotides have been exchanged according to the mt-tRNA sequence, nucleotide 47 in the variable region has been removed, and D- and T-loops shortened and shaped so that no tertiary interaction can occur. The model has further been submitted to an energy minimization step. (**A**) Structure of the tRNA with emphasis of the core interactions. In the right panel, the CCA-end points toward the reader. (**B**) Detailed views on the individual core interactions. The six tertiary interactions found in classical tRNAs are highlighted in the model, in agreement with the chemical probing data collected herein and conservation of Leontis–Westhof rules in 136 mammalian mt-tRNA^{Asp}. The color code is as follows: A15-U48/magenta; U8–A14–A21/blue; U22–A13–U46/green; A9–U12–U23/yellow; G10–C25–A45/brown; A26–A44/red. Figures were prepared with PyMol (31).

Evolution of mammalian mt-tRNA structures

Mammalian mt-tRNAs are considered as 'bizarre' tRNAs due to skewed nucleotide composition and to important size and sequence variations in the D- and T-loops. Here we show that the 3D structure of human mt-tRNA^{Asp} is based on a core domain made up of the classical set of six tertiary interactions. This tRNA presents also a restricted set of four post-transcriptional modifications, all of classical type, from which m^1A9, m^2G10, Ψ27 stabilize the fold. The L-shaped structure remains unusual in regard to its elbow for which no interactions between the D- and T-loops could be detected. However, neither the contribution of residue 60 in the T-loop nor that of specific magnesium ions (59) could be evaluated. Rules determined for human mt-tRNA^{Asp} can be extended to 136 mammalian mt-tRNAs of the same specificity. Detailed structural properties of 19 mammalian mt-tRNA families of different specificities need to be explored to verify if the observations established herein for tRNA^{Asp} can be generalized, or if on the contrary some tRNAs present alternative tertiary networks. We recall that serine specific tRNAs do possess alternate networks (8–10). The recent crystal structure of pyrrolysine specific tRNA from *Desulfitobacterium hafniense* features unprecedented tertiary interactions (66). These are likely valid for the mt-tRNA$^{Ser(UCN)}$ which shares very similar typical secondary structure characteristics (8,9).

The size and sequence degeneracy observed for mammalian mt-tRNA D- and T-loops parallels the functional degeneracy observed for aminoacylation identity sets, restricted in number as compared to other tRNAs (14,67,68). Interestingly, local mutation of aspartyl-tRNA synthetase in response to the loss of the major identity element G73 is an explicit demonstration of an adaptation in a complementary partnership (14). More generally, it is observed that mt-DNA encoded RNA degeneracy is compensated for by adaptation of partner macromolecules belonging to the translational machinery. An extended elongation factor exists specifically for the D-stem deprived tRNA$^{Ser(AGY)}$ (69), a highly protein rich mitochondrial ribosome compensates for restricted 12S and 16S rRNA sequences coded by the mt genome (70) and finally, RNaseP is deprived of an RNA moiety but enriched in protein subunits (57).

Mammalian mt-tRNA structures remain to be defined during interaction with e.g. post-transcriptional

modification enzymes, cognate aminoacyl-tRNA synthetases and mito-ribosomal A, P and E-sites. Large plasticity of tRNA structures is required for each of these partnerships when classical tRNAs are considered, as for example with aminoacyl-tRNA synthetases (e.g. 71), tRNA-guanine transglycosylase (72), or during interaction with the ribosome (73,74). Structural knowledge on mammalian mt-tRNAs will also allow for better understanding of the molecular impacts of mutations correlated with neurodegenerative disorders (43,75).

SUPPLEMENTARY DATA

Supplementary Data are available at NAR Online.

ACKNOWLEDGEMENTS

We thank Joëlle Rudinger-Thirion for helpful advice, Richard Giegé for constructive comments on the manuscript and Louis Levinger for english language improvements. We are grateful to Yohei Kirino (University of Pennsylvania) and Yuriko Sakaguchi (University of Tokyo) for providing materials and technical assistance.

FUNDING

Centre National de la Recherche Scientifique (CNRS), Université de Strasbourg, Association Française contre les Myopathies, Action Concertée Incitative (ACI BCMS) (to C.F.); the Ministry of Education, Science, Sports, and Culture of Japan (to Tom,S.); a JSPS Fellowship for Japanese Junior Scientists (to Takeo,S.); the New Energy and Industrial Technology Development Organization (NEDO) (to Tom,S.); and a fellowship from Ministère de l'Enseignement Supérieur et de la Recherche (to M.M.). Funding for open access charge: CNRS, Université de Strasbourg, AFM.

Conflict of interest statement. None declared.

REFERENCES

1. Giegé,R. (2008) Toward a more complete view of tRNA biology. *Nat. Struct. Mol. Biol.*, **15**, 1007–1014.
2. Jühling,F., Mörl,M., Hartmann,R.K., Sprinzl,M., Stadler,P.F. and Pütz,J. (2009) tRNAdb 2009: compilation of tRNA sequences and tRNA genes. *Nucleic Acids Res.*, **37**, D159–D162.
3. Kim,S.H., Suddath,F.L., Quigley,G.J., McPherson,A., Sussman,J.L., Wang,A.H.J., Seeman,N.C. and Rich,A. (1974) Three dimensional tertiary structure of yeast phenylalanine transfer RNA. *Science*, **185**, 435–440.
4. Robertus,J.D., Ladner,J.E., Finch,J.T., Rhodes,D., Brown,R.S., Clarck,B.F.C. and Klug,A. (1974) Correlation between three-dimensional structure and chemical reactivity of transfer RNA. *Nucleic Acids Res.*, **1**, 927–932.
5. Giegé,R., Puglisi,J.D. and Florentz,C. (1993) tRNA structure and aminoacylation efficiency. *Prog. Nucleic Acid Res. Mol. Biol.*, **45**, 129–206.
6. Dirheimer,G., Keith,G., Dumas,P. and Westhof,E. (1995) In Söll,D. and RajBhandary,U.L. (eds), *tRNA: Structure, Biosynthesis, and Function*. American Society for Microbiology Press, Washington DC, pp. 93–126.
7. Helm,M., Brulé,H., Friede,D., Giegé,R., Pütz,J. and Florentz,C. (2000) Search for characteristic structural features of mammalian mitochondrial tRNAs. *RNA*, **6**, 1356–1379.
8. Yokogawa,T., Watanabe,Y., Kumazawa,Y., Ueda,T., Hirao,I., Miura,K. and Watanabe,K. (1991) A novel cloverleaf structure found in mammalian mitochondrial $tRNA^{Ser(UCN)}$. *Nucleic Acids Res.*, **19**, 6101–6105.
9. Hayashi,I., Kawai,G. and Watanabe,K. (1998) Higher-order structure and thermal instability of bovine mitochondrial $tRNA^{Ser}_{UGA}$ investigated by proton NMR spectroscopy. *J. Mol. Biol.*, **284**, 57–69.
10. Hayashi,I., Yokogawa,T., Kawai,G., Ueda,T., Nishikawa,K. and Watanabe,K. (1997) Assignment of imino proton signals of G-C base pairs and magnesium ion binding: an NMR study of bovine mitochondrial $tRNA^{Ser}_{GCU}$ lacking the entire D arm. *J. Biochem.*, **121**, 1115–1122.
11. Leehey,M.A., Squassoni,C.A., Friederich,M.W., Mills,J.B. and Hagerman,P.J. (1995) A noncanonical tertiary conformation of a human mitochondrial transfer RNA. *Biochemistry*, **34**, 16235–16239.
12. Frazer-Abel,A.A. and Hagerman,P.J. (1999) Determination of the angle between the acceptor and anticodon stems of a truncated mitochondrial tRNA. *J. Mol. Biol.*, **285**, 581–593.
13. Wakita,K., Watanabe,Y.-I., Yokogawa,T., Kumazawa,Y., Nakamura,S., Ueda,T., Watanabe,K. and Nishikawa,K. (1994) Higher-order structure of bovine mitochondrial $tRNA^{Phe}$ lacking the 'conserved' GG and TΨCG sequences as inferred by enzymatic and chemical probing. *Nucleic Acids Res.*, **22**, 347–353.
14. Fender,A., Sauter,C., Messmer,M., Pütz,J., Giegé,R., Florentz,C. and Sissler,M. (2006) Loss of a primordial identity element for a mammalian mitochondrial aminoacylation system. *J. Biol. Chem.*, **281**, 15980–15986.
15. Kirino,Y., Yasukawa,T., Ohta,S., Akira,S., Ishihara,K., Watanabe,K. and Suzuki,T. (2004) Codon-specific translational defect caused by a wobble modification deficiency in mutant tRNA from a human mitochondrial disease. *Proc. Natl Acad. Sci. USA*, **101**, 15070–15075.
16. Suzuki,T. and Suzuki,T. (2007) Chaplet column chromatography: isolation of a large set of individual RNAs in a single step. *Methods Enzymol.*, **425**, 231–239.
17. Suzuki,T., Ikeuchi,Y., Noma,A., Suzuki,T. and Sakaguchi,Y. (2007) Mass spectrometric identification and characterization of RNA-modifying enzymes. *Methods Enzymol.*, **425**, 211–229.
18. Mengel-Jørgensen,J. and Kirpekar,F. (2002) Detection of pseudouridine and other modifications in tRNA by cyanoethylation and MALDI mass spectrometry. *Nucleic Acids Res.*, **30**, e135.
19. Yokogawa,T., Kumazawa,Y., Miura,K.-I. and Watanabe,K. (1989) Purification and characterization of two serine isoacceptor tRNAs from bovine mitochondria by using a hybridization assay method. *Nucleic Acids Res.*, **17**, 2623–2638.
20. Helm,M., Florentz,C., Chomyn,A. and Attardi,G. (1999) Search for differences in post-transcriptional modification patterns of mitochondrial DNA-encoded wild-type and mutant human $tRNA^{Lys}$ and $tRNA^{Leu(UUR)}$. *Nucleic Acids Res.*, **27**, 756–763.
21. Bonnefond,L., Fender,A., Rudinger-Thirion,J., Giegé,R., Florentz,C. and Sissler,M. (2005) Towards the full set of human mitochondrial aminoacyl-tRNA synthetases: characterization of AspRS and TyrRS. *Biochemistry*, **44**, 4805–4816.
22. Fechter,P., Rudinger,J., Giegé,R. and Théobald-Dietrich,A. (1998) Ribozyme processed tRNA transcripts with unfriendly internal promoter for T7 RNA polymerase: production and activity. *FEBS Lett.*, **436**, 99–103.
23. Becker,H.D., Giegé,R. and Kern,D. (1996) Identity of prokaryotic and eukaryotic $tRNA^{Asp}$ for aminoacylation by aspartyl-tRNA synthetase from *Thermus thermophilus*. *Biochemistry*, **35**, 7447–7458.
24. Helm,M., Brulé,H., Degoul,F., Cepanec,C., Leroux,J.-P., Giegé,R. and Florentz,C. (1998) The presence of modified nucleotides is required for cloverleaf folding of a human mitochondrial tRNA. *Nucleic Acids Res.*, **26**, 1636–1643.
25. Peattie,D.A. and Gilbert,W. (1980) Chemical probes for higher-order structure in RNA. *Proc. Natl Acad. Sci. USA*, **77**, 4679–4682.
26. Bonnefond,L., Florentz,C., Giegé,R. and Rudinger-Thirion,J. (2008) Decreased aminoacylation in pathology-related mutants of

mitochondrial tRNA^{Tyr} is associated with structural perturbations in tRNA architecture. *RNA*, **14**, 641–648.
27. Eiler,S., Dock-Bregeon,A.C., Moulinier,L., Thierry,J.-C. and Moras,D. (1999) Synthesis of aspartyl-tRNA^{Asp} in *Escherichia coli*-a snapshot of the second step. *EMBO J.*, **18**, 6532–6541.
28. Kleywegt,G.J., Zou,J.Y., Kjeldgaard,M. and Jones,T.A. (2001) In Rossmann,M.G. and Arnold,E. (eds), *International Tables for Crystallography*. F. Crystallography of Biological Macromolecules, Chapter 17.11. Kluwer Academic, Dordrecht (The Netherlands, pp. 353–356, 366–367.
29. Jossinet,F. and Westhof,E. (2005) Sequence to Structure (S2S): display, manipulate and interconnect RNA data from sequence to structure. *Bioinformatics*, **21**, 3320–3321.
30. Brünger,A.T., Adams,P.D., Clore,G.M., DeLano,W.L., Gros,P., Grosse-Kunstleve,R.W., Jiang,J.S., Kuszewski,J., Nilges,M., Pannu,N.S. *et al.* (1998) Crystallography and NMR system: a new software suite for macromolecular structure determination. *Acta Cryst.*, **D54**, 905–921.
31. DeLano,W.L. (2002) Delano Scientific (http://www.pymol.org). Delano Scientific, San Carlos, CA, USA.
32. Pütz,J., Dupuis,B., Sissler,M. and Florentz,C. (2007) Mamit-tRNA, a database of mammalian mitochondrial tRNA primary and secondary structures. *RNA*, **13**, 1184–1190.
33. Messmer,M., Gaudry,A., Sissler,M. and Florentz,C. (2009) Pathology-related mutation A7526G (A9G) helps in the understanding of the 3D structural core of human mitochondrial tRNA^{Asp}. *RNA*, **15**, 1462–1468.
34. Chen,E.Y. and Roe,B.A. (1980) Structural comparison of human, bovine, rat, and Walker 256 carcinosarcoma asparaginyl-tRNA. *Biochim. Biophys. Acta.*, **610**, 272–284.
35. Ehresmann,C., Baudin,F., Mougel,M., Romby,P., Ebel,J.-P. and Ehresmann,B. (1987) Probing the structure of RNAs in solution. *Nucleic Acids Res.*, **15**, 9109–9128.
36. Giegé,R., Helm,M. and Florentz,C. (1999) In Söll,D., Nishimura,S. and Moore,P. (eds), *Prebiotic Chemistry, Molecular Fossils, Nucleosides, and RNA,* Vol. 6. Pergamon, Oxford, pp. 63–80.
37. Brunel,C. and Romby,P. (2000) Probing RNA structure and RNA–ligand complexes with chemical probes. *Methods Enzymol.*, **318**, 3–21.
38. Sohm,B., Frugier,M., Brulé,H., Olszak,K., Przykorska,A. and Florentz,C. (2003) Towards understanding human mitochondrial leucine aminoacylation identity. *J. Mol. Biol.*, **328**, 995–1010.
39. Steinberg,S. and Cedergren,R. (1994) Structural compensation in atypical mitochondrial tRNAs. *Nature Struct. Biol.*, **1**, 507–510.
40. Steinberg,S., Gautheret,D. and Cedergren,R. (1994) Fitting the structurally diverse animal mitochondrial tRNAs^{Ser} to common three-dimensional constraints. *J. Mol. Biol.*, **236**, 982–989.
41. Steinberg,S., Leclerc,F. and Cedergren,R. (1997) Structural rules and conformational compensations in the tRNA L-form. *J. Mol. Biol.*, **266**, 269–282.
42. Leontis,N.B., Stombaugh,J. and Westhof,E. (2002) The non-Watson-Crick base pairs and their associated isostericity matrices. *Nucleic Acids Res.*, **30**, 3497–3531.
43. Florentz,C., Sohm,B., Tryoen-Tóth,P., Pütz,J. and Sissler,M. (2003) Human mitochondrial tRNAs in health and disease. *Cell Mol. Life Sci.*, **60**, 1356–1375.
44. Levinger,L., Mörl,M. and Florentz,C. (2004) Mitochondrial tRNA 3' end metabolism and human disease. *Nucleic Acids Res.*, **32**, 5430–5441.
45. Helm,M., Giegé,R. and Florentz,C. (1999) A Watson-Crick base-pair disrupting methyl group (m^{1}A9) is sufficient for cloverleaf folding of human mitochondrial tRNA^{Lys}. *Biochemistry*, **38**, 13338–13346.
46. Sissler,M., Helm,M., Frugier,M., Giegé,R. and Florentz,C. (2004) Aminoacylation properties of pathology-related variants of human mitochondrial tRNA^{Lys} variants. *RNA*, **10**, 841–853.
47. Voigts-Hoffmann,F., Hengesbach,M., Kobitski,A.Y., van Aerschot,A., Herdewijn,P., Nienhaus,G.U. and Helm,M. (2007) A methyl group controls conformational equilibrium in human mitochondrial tRNA^{Lys}. *J. Am. Chem. Soc.*, **129**, 13382–13383.
48. Kobitski,A.Y., Hengesbach,M., Helm,M. and Niehaus,G.U. (2008) Sculpting an RNA conformational energy landscape by a methyl group modification – a single -molecule FRET study. *Angew. Chem. Int. Ed. Engl.*, **47**, 4326–4330.
49. Levinger,L., Giegé,R. and Florentz,C. (2003) Pathology-related substitutions in human mitochondrial tRNA^{Ile} reduce precursor 3′-end processing efficiency *in vitro*. *Nucleic Acids Res.*, **31**, 1904–1912.
50. Wittenhagen,L.M., Roy,M.D. and Kelley,S.O. (2003) The pathogenic U3271C human mitochondrial tRNA$^{Leu(UUR)}$ mutation disrupts a fragile anticodon stem. *Nucleic Acid Res.*, **31**, 596–601.
51. Roy,M.D., Wittenhagen,L.M. and Kelley,S.O. (2005) Structural probing of a pathogenic tRNA dimer. *RNA*, **11**, 254–260.
52. Sohm,B., Sissler,M., Park,H., King,M.P. and Florentz,C. (2004) Recognition of human mitochondrial tRNA$^{Leu(UUR)}$ by its cognate leucyl-tRNA synthetase. *J. Mol. Biol.*, **339**, 17–29.
53. Anderson,S., Bankier,A.T., Barrel,B.G., de Bruijn,M.H.L., Coulson,A.R., Drouin,J., Eperon,J.C., Nierlich,D.P., Roe,B.A., Sanger,F. *et al.* (1981) Sequence and organization of the human mitochondrial genome. *Nature*, **290**, 457–465.
54. Madore,E., Florentz,C., Giegé,R., Sekine,S.-i., Yokoyama,S. and Lapointe,J. (1999) Effect of modified nucleotides on *Escherichia coli* tRNA^{Glu} structure and on its aminoacylation by glutamyl-tRNA synthetase; predominant and distinct roles of the mnm^5 and s^2 modifications of U34. *Eur. J. Biochem.*, **266**, 1128–1135.
55. Grosjean,H. (2009) In Grosjean,H. (ed.), *DNA and RNA Modification Enzymes: Structure, Mechanisms, Functions and Evolution,* Vol. 1. Landes BioScience, USA, pp. 1–18.
56. Sakurai,M., Ohtsuki,T. and Watanabe,K. (2005) Modification at position 9 with 1-methyladenosine is crucial for structure and function of nematode mitochondrial tRNAs lacking the entire T-arm. *Nucleic Acids Res.*, **33**, 1653–1661.
57. Holzmann,J., Frank,P., Loffler,E., Bennett,K.L., Gerner,C. and Rossmanith,W. (2008) RNaseP without RNA: identification and functional reconstitution of the human mitochondrial tRNA processing enzyme. *Cell*, **135**, 462–474.
58. Auffinger,P. and Westhof,E. (1998) In Grosjean,H. and Benne,R. (eds), *Modification and Editing of RNA*. ASM Press, Washington, pp. 103–112.
59. Jones,C.I., Spencer,A.C., Hsu,J.L., Spremulli,L.L., Martinis,S.A., DeRider,M. and Agris,P.F. (2006) A counterintuitive Mg^{2+}-dependent and modification-assisted functional folding of mitochondrial tRNAs. *J. Mol. Biol.*, **362**, 771–786.
60. Bykhovskaya,Y., Casas,K., Mengesha,E., Inbal,A. and Fischel-Ghodsian,N. (2004) Missense mutation in pseudouridine synthase 1 (PUS1) causes mitochondrial myopathy and sideroblastic anemia (MLASA). *Am. J. Hum. Genet.*, **74**, 1303–1308.
61. Yokoyama,S. and Nishimura,S. (1995) In Söll,D. and RajBhandary,U. (eds), *tRNA: Structure, Biosynthesis, and Function*. ASM, Washington DC, pp. 207–223.
62. Gustilo,E.M., Vendeix,F.A. and Agris,P.F. (2008) tRNA's modifications bring order to gene expression. *Curr Opin Microbiol.*, **11**, 134–140.
63. Grosjean,H. (2009) *DNA and RNA Modification Enzymes: Structure, Mechanisms, Functions and Evolution*. Landes BioScience, USA.
64. Hayrapetyan,A., Seidu-Larry,S. and Helm,M. (2009) In Grosjean,H. (ed.), *DNA and RNA Modification Enzymes: Comparative Structure, Mechanism, Functions, Cellular Interactions and Evolution,* chapter 37. Landes BioSciences, USA.
65. Romby,P., Moras,D., Dumas,P., Ebel,J.-P. and Giegé,R. (1987) Comparison of the tertiary structure of yeast tRNA^{Asp} and tRNA^{Phe} in solution. Chemical modification study of the bases. *J. Mol. Biol.*, **195**, 193–204.
66. Nozawa,K., O'Donoghue,P., Gundllapalli,S., Araiso,Y., Ishitani,R., Umehara,T., Soll,D. and Nureki,O. (2009) Pyrrolysyl-tRNA synthetase-tRNA(Pyl) structure reveals the molecular basis of orthogonality. *Nature*, **457**, 1163–1167.
67. Lenhard,B., Orellana,O., Ibba,M. and Weygand-Durasevic,I. (1999) tRNA recognition and evolution of determinants in seryl-tRNA synthesis. *Nucleic Acids Res.*, **27**, 721–729.
68. Bonnefond,L., Frugier,M., Giegé,R. and Rudinger-Thirion,J. (2005) Human mitochondrial TyrRS disobeys the tyrosine idenity rules. *RNA*, **11**, 558–562.
69. Ohtsuki,T., Sato,A., Watanabe,Y.-I. and Watanabe,K. (2002) A unique serine-specific elongation factor Tu found in nematode mitochondria. *Nat. Struct. Biol.*, **9**, 669–673.

70. Sharma,M.R., Koc,E.C., Datta,P.P., Booth,T.M., Spremulli,L.L. and Agrawal,R.K. (2003) Structure of the mammalian mitochondrial ribosome reveals an expanded functional role for its component proteins. *Cell*, **115**, 97–108.
71. Ruff,M., Krishnaswamy,S., Boeglin,M., Poterszman,A., Mitschler,A., Podjarny,A., Rees,B., Thierry,J.C. and Moras,D. (1991) Class II aminoacyl transfer RNA synthetases: crystal structure of yeast aspartyl-tRNA synthetase complexed with $tRNA^{Asp}$. *Science*, **252**, 1682–1689.
72. Ishitani,R., Nureki,O., Nameki,N., Okada,N., Nishimura,S. and Yokoyama,S. (2003) Alternative tertiary structure of tRNA for recognition by a posttranscriptional modification enzyme. *Cell*, **113**, 383–394.
73. Yusupov,M.M., Yusupova,G.Z., Baucom,A., Lieberman,K., Earnest,T.N., Cate,J.H.D. and Noller,H.F. (2001) Crystal structure of the ribosome at 5.5Å resolution. *Science*, **292**, 883–896.
74. Selmer,M., Dunham,C.M., Murphy,F.V. IV, Weixlbaumer,A., Petry,S., Kelley,A.C., Weir,J.R. and Ramakrishnan,V. (2006) Structure of the 70S ribosome complexed with mRNA and tRNA. *Science*, **313**, 1935–1942.
75. Wittenhagen,L.M. and Kelley,S.O. (2003) Impact of disease-related mitochondrial mutations on tRNA structure and function. *TIBS*, **28**, 605–611.
76. Mcluckey,S.A., Vanberkel,G.J. and Glish,G.L. (1992) Tandem mass-spectrometry of small, multiply charged oligonucleotides. *J. Am. Soc. Mass Spectrometry*, **3**, 60–70.